

Ensemble manifold based regularized multi-modal graph convolutional network for cognitive ability prediction

Gang Qu, Li Xiao, Wenxing Hu, Kun Zhang, Vince D. Calhoun, *Fellow, IEEE*, Yu-Ping Wang, *Senior Member, IEEE*

Abstract—Objective: Multi-modal functional magnetic resonance imaging (fMRI) can be used to make predictions about individual behavioral and cognitive traits based on brain connectivity networks. **Methods:** To take advantage of complementary information from multi-modal fMRI, we propose an interpretable multi-modal graph convolutional network (MGCN) model, incorporating the fMRI time series and the functional connectivity (FC) between each pair of brain regions. Specifically, our model learns a graph embedding from individual brain networks derived from multi-modal data. A manifold-based regularization term is then enforced to consider the relationships of subjects both within and between modalities. Furthermore, we propose the gradient-weighted regression activation mapping (Grad-RAM) and the edge mask learning to interpret the model, which is used to identify significant cognition-related biomarkers. **Results:** We validate our MGCN model on the Philadelphia Neurodevelopmental Cohort to predict individual wide range achievement test (WRAT) score. Our model obtains superior predictive performance over GCN with a single modality and other competing approaches. The identified biomarkers are cross-validated from different approaches. **Conclusion and Significance:** This paper develops a new interpretable graph deep learning framework for cognitive ability prediction, with the potential to overcome the limitations of several current data-fusion models. The results demonstrate the power of MGCN in analyzing multi-modal fMRI and discovering significant biomarkers for human brain studies.

Index Terms—fMRI, functional connectivity, graph convolutional networks, interpretable deep learning, multi-modal deep learning

I. INTRODUCTION

Functional magnetic resonance imaging (fMRI) provides a non-invasive, high-resolution technique for observing the low-frequency fluctuation in blood-oxygenation-level-dependent (BOLD) signals to characterize the metabolism of the human

brain. Recent evidence [1]–[3] suggests that multiple fMRI datasets contain complementary information and can predict individual variations in behavioral and cognitive traits better than using a single dataset. Numerous data fusion methods have been developed to integrate multiple paradigms of fMRI. For instance, ICA-based approaches [4], [5] were proposed by Calhoun *et al.* and Sui *et al.* to analyze the joint information from multiple fMRI paradigms. Jie *et al.* [6] and Zhu *et al.* [7] proposed manifold regularized multi-task learning models to describe the subject-subject and the response-response relationships. These models were further extended by Xiao *et al.* [8] to incorporate the relation information both within and between modalities. These approaches are typically based on linear models without considering complex nonlinear relationship between these data.

Recently, there has been growing interest in applying graph deep learning models [9] to various fMRI studies such as disease prediction [10] and biomarkers identification [11]. Compared with conventional deep learning models, graph deep learning model directly takes graph-structured data as the input and is therefore ideal for brain network analysis. To this end, we propose an interpretable end-to-end multi-modal graph convolution network (MGCN) framework to integrate multiple paradigms of fMRI, which incorporates different levels of information, from the signal in each brain region of interest (ROI) and the functional connectivity (FC) [12] between each pair of ROIs to subject-subject and paradigm-paradigm relationships. The individual brain network is regarded as a graph represented using the ROIs as nodes and the FCs between each pair of ROIs as edges to predict the individual phenotypes. Specifically, the node feature on the graph is defined as the fMRI time-series of each ROI and the edge is defined as the FC between each pair of ROIs measured with Pearson correlation. We use the feature map learned from the intermediate layer of the network as the graph embedding to calculate individual similarities within and between paradigms. A manifold based regularization term is then enforced on the loss function to incorporate relationships between subjects. Our end-to-end MGCN model is then used for the phenotype prediction and biomarker identification. However, the decision mechanism behind the end-to-end neural network makes the model difficult to interpret. Inspired by the works of [13]–[15], we propose the gradient-based method, namely Gradient-weighted Regression Activation Mapping (Grad-RAM) to track each node’s gradient and generate an activation map

This work was supported in part by NIH under Grants R01 GM109068, R01 MH104680, R01 MH107354, P20 GM103472, R01 REB020407, R01 EB006841, and 2U54MD007595, and in part by NSF under Grant #1539067. (Corresponding author: Yu-Ping Wang.)

Yu-Ping Wang* is with the Biomedical Engineering Department, Tulane University, New Orleans, LA 70118, USA. (e-mail: wyp@tulane.edu).

Kun Zhang is with the Department of Computer Science Department, Xavier University of Louisiana, New Orleans, LA 70125, USA. (e-mail: kzhang@xula.edu).

Vince D. Calhoun is with the Tri-Institutional Center for Translational Research in Neuroimaging and Data Science (TReNDS) (Georgia State University, Georgia Institute of Technology, Emory University), Atlanta, GA, USA (e-mail: vcalhoun@gsu.edu).

Gang Qu, Li Xiao, and Wenxing Hu are with the Biomedical Engineering Department, Tulane University, New Orleans, LA 70118, USA. (e-mail: gqu1@tulane.edu).

to identify significant nodes (ROIs) in the prediction task. Moreover, to interpret the model at the connection level, we propose the edge mask learning to learn a matrix pattern and show the significance of each edge (FC). The L_1 regularization is applied to analyze the pattern with different sparsity thresholds.

We validate our proposed framework using the Philadelphia Neurodevelopmental Cohort (PNC) [16], [17]. Two fMRI paradigms, including a memory task and an emotion cognition task, referred as modalities here, are simultaneously used for phenotype prediction and biomarkers identification. The Wide Range Achievement Test (WRAT) [18] score is used as the predicted phenotype, which measures individual ability in reading, spelling, comprehending, and solving mathematical problems. In the experiment, we first compare the predictive performance of our model with the other competing models. The results demonstrate that our proposed framework yields superior predictive performance. In addition, we interpret the framework and identify significant human cognition-related biomarkers in both ROI and FC levels using Grad-RAM and edge mask learning, respectively. The results from two interpretation strategies provide different views to understand the human brain's cognitive function. We then analyze the functional networks (FNs) based on the identification results and provide the relevant literature to support our findings.

We organize the rest of the paper as follows. In Section II, we briefly review the graph convolutional networks, our proposed multi-modal graph neural network, and the details of Grad-RAM and edge mask learning. We then perform the experiment on PNC and describe the experimental results with some discussions in Section III. We conclude this paper in Section IV. We list the commonly used notations in Table I for convenience.

TABLE I
COMMONLY USED NOTATIONS.

Notation	Definition
\mathcal{G}	a graph
$\ \mathbf{B}\ _1$	the sum of the absolute values of all entries of matrix \mathbf{B}
$\mathbf{B}^{(i,j)}$	the (i,j) th entry of matrix \mathbf{B}
$\mathbf{B}_n^{(m)}$	matrix \mathbf{B} for the n th subject in the m th modality
\mathbf{H}^l	the feature map in the l th layer of the framework
N	number of subjects
Q	number of nodes (ROIs) in brain networks
C	number of feature channels for the graph embedding
\odot	the Hadamard product
\mathbf{X}	the fMRI time-series

II. METHODS

A. Graph convolutional network

Graph convolutional network (GCN) uses networks as the input. Given a graph \mathcal{G} , let \mathbf{U} be the eigenvector matrix of the normalized graph Laplacian:

$$\mathbf{L}_{\text{norm}} := \mathbf{I} - \mathbf{D}^{-\frac{1}{2}} \mathbf{A} \mathbf{D}^{-\frac{1}{2}}, \quad (1)$$

where \mathbf{I} , \mathbf{D} , and \mathbf{A} are the identity matrix, the degree matrix, and the adjacency matrix, respectively. The graph convolution

between the graph signal \mathbf{x} and the filter g_θ in the spatial domain [19] can be defined as

$$g_\theta * \mathbf{x} = \mathbf{U} g_\theta \mathbf{U}^T \mathbf{x}, \quad (2)$$

where $\mathbf{x} \in \mathbb{R}^d$ is the input vector for each node.

To reduce computational complexity, graph convolution can be further simplified using Chebyshev polynomials up to the K th order into

$$g_\theta * \mathbf{x} = \sum_{k=0}^K \theta'_k T_k(\tilde{\mathbf{L}}), \quad (3)$$

where $\tilde{\mathbf{L}} = 2\mathbf{L}_{\text{norm}}/\lambda_{\max} - \mathbf{I}$, and λ_{\max} refers to the largest eigenvalue of \mathbf{L}_{norm} , and T_k is the K th order Chebyshev polynomial. The number of free parameters for graph convolution can be further constrained [9] using renormalization. Therefore, the GCN layer can be rewritten as

$$\mathbf{H}^{l+1} = \phi^l(\tilde{\mathbf{D}}^{-\frac{1}{2}} \tilde{\mathbf{A}} \tilde{\mathbf{D}}^{-\frac{1}{2}} \mathbf{H}^l \Theta^l) \quad (4)$$

where $\tilde{\mathbf{A}} = \mathbf{A} + \mathbf{I}$, $\tilde{\mathbf{D}}$ is the degree matrix with respect to $\tilde{\mathbf{A}}$, and ϕ^l , \mathbf{H}^l and Θ^l are the activation function, the feature map and the weight matrix for the l th layer, respectively.

B. Multi-modal graph convolutional networks

We next propose our multi-modal graph convolutional networks (MGCN) to analyze the brain networks derived from multiple modalities. The brain network for each individual is regarded as one graph. The edge is here represented using absolute value of the Pearson correlation coefficient between the time-series on each pair of ROIs. The K-nearest neighbor algorithm is then applied to the adjacency matrix, keeping the largest K values for each row and column and letting the rest be zero. We apply the two-layer GCN to learn the graph embedding for an individual in each modality, i.e.,

$$\mathbf{Z} = \phi^1(\tilde{\mathbf{D}}^{-\frac{1}{2}} \tilde{\mathbf{A}} \tilde{\mathbf{D}}^{-\frac{1}{2}} \phi^0(\tilde{\mathbf{D}}^{-\frac{1}{2}} \tilde{\mathbf{A}} \tilde{\mathbf{D}}^{-\frac{1}{2}} \mathbf{X} \Theta^0) \Theta^1), \quad (5)$$

where \mathbf{X} and \mathbf{Z} are the fMRI time-series and the graph embedding, respectively. Notably, the individuals in the same modality share the same Θ^0 and Θ^1 .

The embeddings of all individuals in the same modality are vectorized and formed into a matrix $\mathbf{Z}^{(m)} = [\text{vec}(\mathbf{Z}_1^{(m)}), \text{vec}(\mathbf{Z}_2^{(m)}), \dots, \text{vec}(\mathbf{Z}_N^{(m)})]^T \in \mathbb{R}^{N \times QC}$. Next, the multi-layer perceptron (MLP) of two dense layers is used to fuse the embeddings from all M modalities for the prediction.

$$\hat{\mathbf{y}} = \text{MLP}(\mathbf{Z}), \quad (6)$$

where $\mathbf{Z} = [\mathbf{Z}^{(1)}; \mathbf{Z}^{(2)}; \dots; \mathbf{Z}^{(M)}] \in \mathbb{R}^{MN \times QC}$, and $\hat{\mathbf{y}} \in \mathbb{R}^N$ is the prediction of WRAT scores for N subjects.

However, the relationships of subjects from different modalities have not been considered yet. For a joint analysis of multiple modalities to boost learning performance, we impose a novel manifold based regularization term, enabling the MGCN to incorporate the relationships between the subjects both within and between multiple modalities. To do so, we first used the Pearson correlation to define the brain network similarity of two subjects in the m th modality as

$$\mathbf{S}_{(i,j)}^{(m)} = |\text{corrcoef}(\text{vec}(\mathbf{A}_i^{(m)}), \text{vec}(\mathbf{A}_j^{(m)}))|, \quad (7)$$

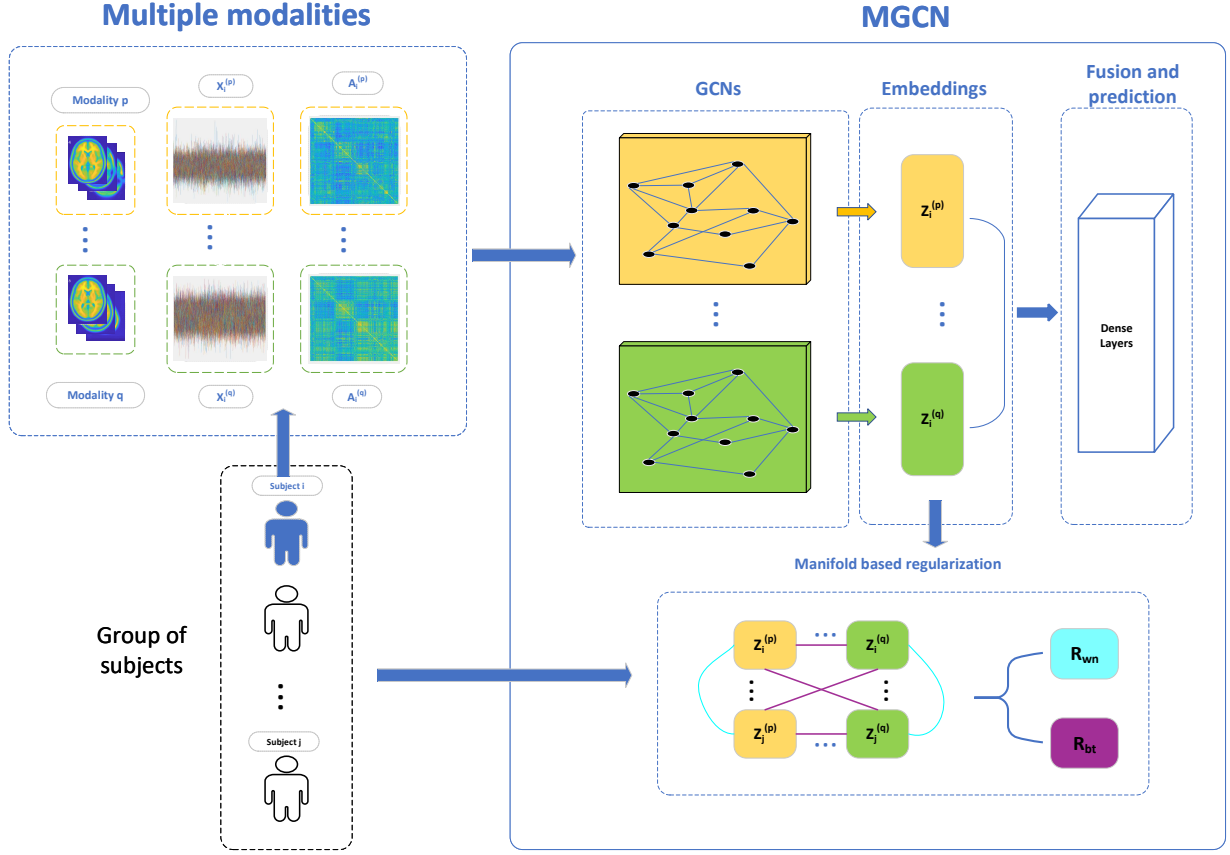


Fig. 1. The flowchart of our proposed framework. The GCN block can learn the graph embeddings from multi-modal. Afterward, the manifold based regularization is calculated to incorporate the relations of subjects within and between modalities. The dense layers fuse the embeddings from different modalities for prediction.

where $S_{(i,j)}^{(m)}$ is the $(i, j)_{th}$ entry of the matrix $S^{(m)} \in \mathbb{R}^{N \times N}$, and here $A_i^{(m)}$ and $A_j^{(m)}$ are the adjacency matrices before applying the K-nearest neighbor algorithm. Then, the similarity of subjects between different modalities can be represented as the product of the similarity matrices in each modality, i.e., $S^{(p)}S^{(q)}$ is the similarity between p_{th} and q_{th} modalities. Our manifold based regularization term is therefore defined as a combination of

$$R_{wn} = \frac{1}{2} \sum_m \sum_{i,j} S_{(i,j)}^{(m)} \|vec(\mathbf{Z}_i^{(m)}) - vec(\mathbf{Z}_j^{(m)})\|_2^2, \quad (8)$$

$$R_{bt} = \frac{1}{2} \sum_{p \neq q} \sum_{i,j} (S^{(p)}S^{(q)})_{(i,j)} \|vec(\mathbf{Z}_i^{(p)}) - vec(\mathbf{Z}_j^{(q)})\|_2^2,$$

where R_{bt} and R_{wn} are used to incorporate the subject-subject relationship within each single modality and between modalities, respectively.

The manifold regularization term fully explores the relationship between subjects, enforcing the model to learn similar embeddings for subjects with high brain structure similarity both within and between modalities. Furthermore, we can write the similarities into a single matrix $S \in \mathbb{R}^{MN \times MN}$

with the regularization parameters,

$$S = \begin{bmatrix} \eta_2 S^{(1)} & \eta_1 S^{(1)} S^{(2)} & \dots & \eta_1 S^{(1)} S^{(M)} \\ \eta_1 S^{(2)} S^{(1)} & \eta_2 S^{(2)} & \dots & \eta_1 S^{(2)} S^{(M)} \\ \vdots & \vdots & \ddots & \vdots \\ \eta_1 S^{(M)} S^{(1)} & \eta_1 S^{(M)} S^{(2)} & \dots & \eta_2 S^{(M)} \end{bmatrix}, \quad (9)$$

where the diagonal elements represent the within modality similarities, and η_1 and η_2 are the regularization parameters of between and within modalities, respectively. Therefore, the regularization term can then be written as

$$R_m = \eta_1 R_{bt} + \eta_2 R_{wn} = \text{trace}(\mathbf{Z}^T \mathbf{L} \mathbf{Z}), \quad (10)$$

where $L = D - S$, and D is the degree matrix of S . The mean square error (MSE) combined with the manifold based regularization term and the L_2 norm on weight matrices is used as the loss function (denoted as *loss*). The workflow of our MGCN framework is shown in Fig.1.

C. Gradient-weighted Regression activation mapping

To interpret the MGCN at the node level, we propose the Gradient-weighted Regression Activation Mapping (Grad-

RAM) to track the gradient of the graph embedding with respect to the prediction value in each modality,

$$\mathbf{G}_{(n,qc)}^{(m)} = \frac{\partial \mathbf{y}_n}{\partial \mathbf{Z}_{(n,qc)}^{(m)}}, \quad (11)$$

where \mathbf{y}_n is the label for the n_{th} subject, $\mathbf{G}^{(m)} \in \mathbb{R}^{N \times QC}$ is the gradient matrix in m_{th} modality, and $\mathbf{Z}_{(n,qc)}^{(m)}$ is the $(n, qc)_{th}$ entry of $\mathbf{Z}^{(m)}$.

Accordingly, using the graph embedding values to be the weights, we defined the Grad-RAM as the product between gradients and the graph embeddings over N subjects.

$$\mathbf{a}_{(q)}^{(m)} = \frac{1}{NC} \text{ReLU} \left(\sum_{n=1, c=1}^{NC} \mathbf{G}_{(n,qc)}^{(m)} \mathbf{Z}_{(n,qc)}^{(m)} \right), \quad (12)$$

where $\mathbf{a}_{(q)}^{(m)}$ is the Grad-RAM value of the q_{th} ROI in the m_{th} modality. The ReLU function is applied to keep the features with a positive influence on the final prediction. Afterward, we have $\mathbf{a}^{(m)} \in \mathbb{R}^Q$ as the activation map in the ROI level for the m_{th} modality. We used Grad-RAM to visualize the important ROIs for WRAT score prediction.

D. Edge mask learning

We next propose the edge mask learning to interpret our framework at the edge level. In particular, rather than learning explainable patterns for each modality separately, we retrain the model and jointly learn an edge mask matrix for subjects from all modalities. Since only the indirect graph is considered, the edge mask must be symmetric and non-negative, which is defined as

$$\mathcal{M} = \text{ReLU}(\mathbf{V} + \mathbf{V}^T), \quad (13)$$

where the entry of mask \mathcal{M} indicates the weight for each edge, $\mathbf{V} \in \mathbb{R}^{Q \times Q}$ is the matrix we need to optimize, and the ReLU function ensures the elements to be non-negative.

Consequently, the Eq.4 and the loss function can be rewritten as Eq.14 and Eq.15, respectively.

$$\mathbf{H}^{l+1} = \phi^l((\mathcal{M} + \mathbf{I}) \odot (\tilde{\mathbf{D}}^{-\frac{1}{2}} \tilde{\mathbf{A}} \tilde{\mathbf{D}}^{-\frac{1}{2}})) \mathbf{H}^l \Theta^l), \quad (14)$$

$$\hat{loss} = loss + \beta \|\mathcal{M}\|_1, \quad (15)$$

where β is the L_1 regularization parameter to control the sparsity level of the learned mask. Notably, by adding the identity matrix \mathbf{I} to \mathcal{M} , we obtain the identity mapping when $\mathcal{M} = \mathbf{0}$ and guarantee the graph filter will not degrade to the null matrix.

III. EXPERIMENTS

Our framework was validated on the PNC. In this section, we first briefly describe the PNC and the preprocessing of the dataset, and then present our experimental results and discussions.

A. Datasets

The PNC consists of multiple fMRI paradigms acquired from over 800 healthy subjects aged from 8 to 22 years. Two task fMRI data, the emotion cognition task (emoid-fMRI) and working memory task data (nback-fMRI), were used to predict various physiological phenotype. The emoid-fMRI and nback fMRI scan durations were 10.5 minutes (210 TR) and 11.6 minutes (231 TR). When measuring the emoid-fMRI, subjects were asked to identify the face with different emotions like angry, sad, fearful, happy, and label the emotion type. For the nback-fMRI scans, subjects were asked to conduct standard n-back tasks, which were related to working memory and the ability of lexical processing. The WRAT scores were collected from a 1-hour computerized neurocognitive battery (CNB) administered by the PNC, which were regarded as the label to assess individual reading and comprehension ability [20].

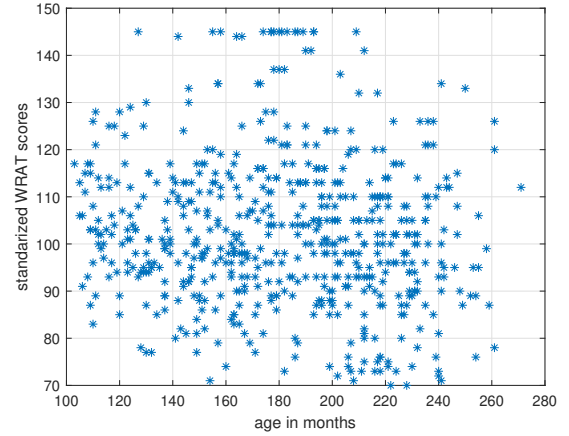


Fig. 2. The scatter plot of WRAT score versus age

All MRI scans were collected on a single 3T Siemens TIM Trio whole-body scanner. We followed similar preprocessing procedures as in [21], [22]. SPM12¹ was used to conduct motion correction, spatial normalization, after which the data were smoothed with a 3mm Gaussian kernel. Multiple regressions were used while the influence of head motion was considered [23]. Then, we applied 264-region parcellation ($Q = 264$) to investigate whole-brain connectivity. As a result, we had 264 ROIs (containing 21,384 voxels) based on the Power coordinates template (sphere radius is 5mm) [24]. We included only subjects with both emoid-fMRI and nback-fMRI resulting in 595 samples. We further investigated potential confounders for the WRAT-fMRI association, including age, gender, and head motion.

- Age: The WRAT-age distribution was shown in Table III. Instead of using the raw WRAT scores, the standardized WRAT scores [20] were considered, e.g., in Fig.2. The grade-based and age-based norms were added to control the age factor and to enhance the interpretation of the test results.
- Gender: The gender-WRAT information was shown in Table III. The mean and standard deviation of WRAT

¹<http://www.fil.ion.ucl.ac.uk/spm/software/spm12/>

TABLE II
THE PREDICTION PERFORMANCE WITH DIFFERENT MODELS.

Model	Modalities	RMSE(mean \pm std)	p-value	MAE(mean \pm std)	p-value
GCN	emoid fMRI	15.6924 \pm 0.9912	6.222e-04	12.3965 \pm 0.7972	1.847e-04
GCN	nback fMRI	15.4335 \pm 0.5867	9.022e-04	12.0440 \pm 0.6688	2.376e-04
MTL	emoid fMRI	16.1742 \pm 0.9283	2.548e-05	12.5691 \pm 0.6846	2.101e-05
MTL	nback fMRI	16.2187 \pm 0.9576	2.501e-05	12.5780 \pm 0.7190	2.714e-05
M2TL	emoid fMRI	15.9967 \pm 0.8947	5.461e-05	12.5425 \pm 0.5454	6.681e-06
M2TL	nback fMRI	15.0807 \pm 0.8902	0.0136	11.6161 \pm 0.7958	0.0362
NM2TL	emoid fMRI	15.0320 \pm 0.7965	0.0125	11.6963 \pm 0.5853	0.0083
NM2TL	nback fMRI	15.0310 \pm 0.7955	0.0125	11.6885 \pm 0.5771	0.0085
MLP	emoid fMRI & nback fMRI	15.1341 \pm 0.5883	0.0023	11.9957 \pm 0.9259	0.0059
MVGCN	emoid fMRI & nback fMRI	14.9858 \pm 0.9031	0.0246	11.7140 \pm 0.7608	0.0167
MGCN*	emoid fMRI & nback fMRI	14.8267 \pm 0.6618	0.0285	11.5339 \pm 0.6226	0.0337
MGCN	emoid fMRI & nback fMRI	14.0889 \pm 0.7222	-	10.8878 \pm 0.6339	-

¹ p-values were calculated by t-test between the regression performance for repeated experiments of our MGCN model and other competing models; std denotes the standard deviation.

² * the MGCN without the manifold based regularization term.

TABLE III
GENDER-WRAT INFORMATION.

property\group	male	female	Total
number of subjects	271	324	595
mean WRAT scores	104.20	101.44	102.30
std WRAT scores	16.61	15.14	15.87

scores of males and females are close. As a result, we consider the gender impact on WRAT scores is negligible..

- Head motion: We collected 6 rigid body motion parameters(3 translations along x, y, z axes, and 3 rotations around x, y, z axes). The framewise displacement (FD) of head position, which is defined as the sum of the absolute values of the derivatives of those 6 rigid body motion parameters [25], was then calculated. Next, we tested the hypothesis that there is no relationship between the WRAT scores and the mean FD using the matrix of Pearson correlation coefficients. The respective p-values were 0.3029 for emoid-fMRI and 0.3599 for nback-fMRI. No significant relationships between the head motion and WRAT scores were observed at 0.05 level.

In addition, the mean-centering was applied to the labels using the mean WRAT scores of training samples. For each subject, the signal matrices were then formatted as $\mathbf{X}_{emoid} \in \mathbb{R}^{264 \times 210}$ of the emoid-fMRI and $\mathbf{X}_{nback} \in \mathbb{R}^{264 \times 231}$ of the nback-fMRI.

B. Experimental setup

We randomly split the data into training, validation, and testing sets with the ratio of 70%, 10%, 20%, respectively. We trained the model on the training set and tuned the hyperparameters on the validation set. The root mean square error (RMSE) and mean absolute error (MAE) between the predicted and observed WRAT scores in the test set were calculated. The bootstrap analysis was utilized to measure and compare models' performance, reducing sampling bias with

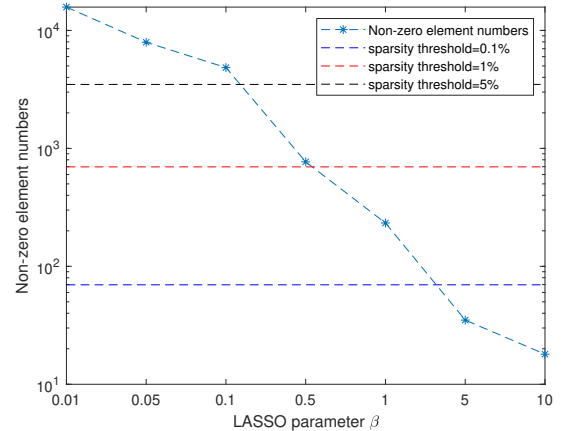


Fig. 3. The sparsity of edge mask with respect to the L_1 regularization parameter

10 repeated experiments. For each experiment, we repeated the dataset splitting, model training, and testing processes. Besides, we compared the results of repeated experiments collected from our proposed model with other approaches, and reported the p-values of the pairwise t-test to show the statistically significant improvement.

C. Results

1) *Hyperparameter selection*: The hyperparameters of the MGCN model were tuned on validation sets through the random search [27]. In addition, the L_2 regularization term with a parameter $1e - 4$ was enforced on weight matrices to avoid overfitting. Consequently, for MGCN, we set the $K = 10$ for K-nearest neighbors and trained the model for up to 1000 epochs and a learning rate of $1e - 5$ with early stop. The two-layer GCNs in Eq.5 were used for graph embedding. We set the numbers of feature channels to be 128 and 32, and the activation functions to be *ReLU* and *Sigmoid* for the first and the second GCN layer, respectively. Next, two dense layers with respective 1024 and 2048 neurons and with

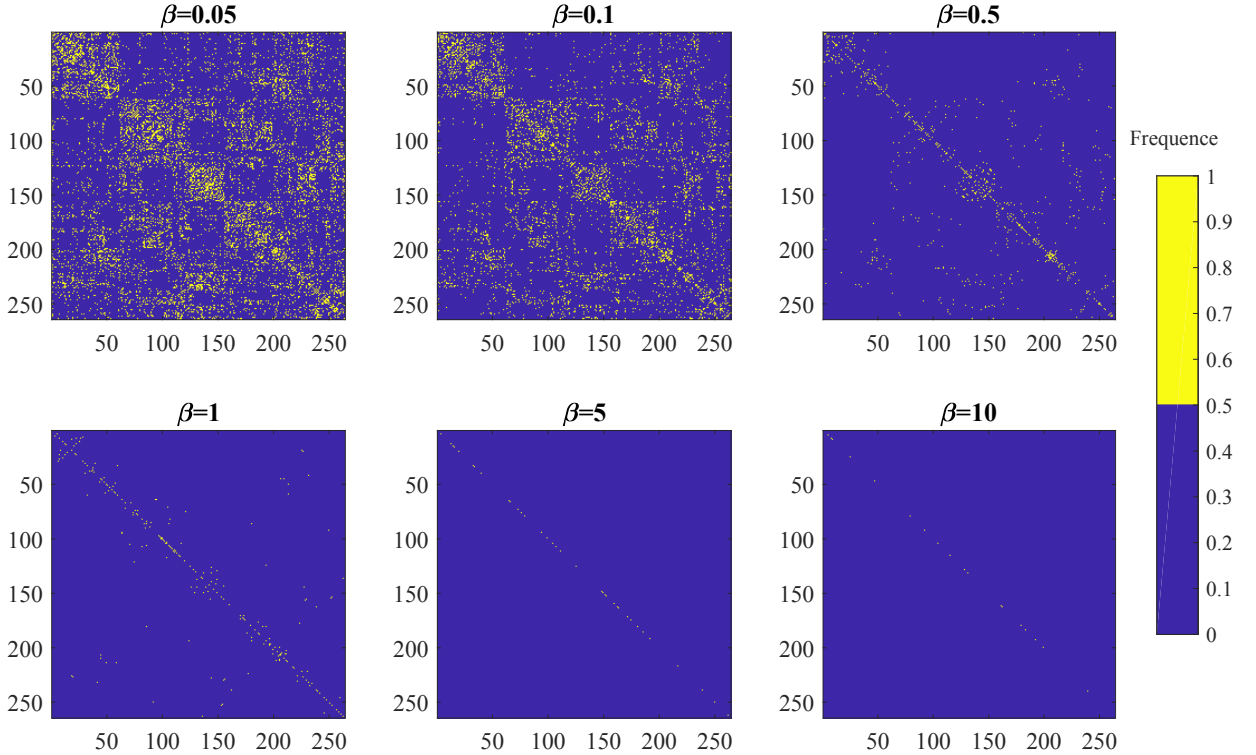


Fig. 4. The edge masks learned with different L_1 regularization parameters

ReLU activation functions were used to merge the graph embeddings from two modalities, as in Eq.6. The manifold based regularization parameters in Eq.10 were tuned in the range from 10^{-5} to 10^{-2} .

We here reported the running time in the training process and used GCN with the same graph convolution layers for a single modality as the baseline to measure the extra computational cost. The results showed that MGCN (0.2132 ± 0.0152 secs) took almost three times more time than GCN (0.0796 ± 0.0049 secs) per iteration due to more complicated network structure and the calculation of manifold based regularization.

2) *Performance in comparison to other methods:* We compared our model with the Multi-task learning model [28], Manifold regularized multi-task learning (M2TL) [7], New Manifold regularized multi-task learning (NM2TL) [8], GCN with single paradigm fMRI, MLP, multi-view GCN (MVGCN) [29], and MGCN without the manifold based regularization term in Eq.10.

- The single modal GCN was validated using emoid-fMRI or nback-fMRI with the same hyperparameter selection as the GCN part of MGCN.
- For the MTL, M2TL, NM2TL, the hyperparameters were tuned using the random search. Notably, a different strategy in subjects selection was applied in [8], in which the subjects were selected based on the age threshold for MTL, M2TL, and NM2TL. For the MLP, we used the same network structure as the MGCN.

- For the MVGCN, the network structure and hyperparameter settings were used as the GCN part of our MGCN. The main differences were that MVGCN applied the view pooling [29] to fuse the embedded feature matrices from different modalities without manifold based regularization term.

The predictive performance was evaluated using bootstrap analysis on 10 repeated experiments. We showed the comparison results in Table II, from which we can see that our model achieved superior RMSE and MAE over other approaches. Furthermore, enforcing the manifold based regularization term in MGCN improves prediction performance, suggesting that our model can extract more discriminative features by incorporating subjects' relationships within and between different modalities.

D. Model explanation and biomarker identification

We next interpreted our model and identified the cognition-related biomarkers at the ROI, FC, and FN levels. The following abbreviations of the FNs were used: Sensory/somatomotor network (SMN), Auditory network (AUD), cingulo-opercular task control Network (CNG), default mode network (DMN), visual network (VIS), Fronto-parietal Task Control (FPN), salience network (SAL), subcortical network (SCT), Ventral attention Network (VTRN), Dorsal attention network (DA), and Cerebellar (CEB).

TABLE IV
THE SELECTED ROIS (TOP 5%)

ROI	emoid-fMRI		
	MNI space ¹	Anatomical region ¹	FN
23	-23 -30 72	Postcentral L	SMN
32	22 -42 69	Postcentral R	SMN
47*	-3 2 53	Supp Motor Area L	CNG
59*	-5 18 34	Cingulum Mid L	CNG
92	8 -48 31	Cingulum Mid R	DMN
101	22 39 39	Frontal Sup R	DMN
112*	-2 38 36	Frontal Sup R	DMN
113*	-3 42 16	Cingulum Ant L	DMN
153*	43 -78 -12	Occipital Inf R	VIS
162*	24 -87 24	Occipital Sup R	VIS
167*	-3 -81 21	Cuneus L	VIS
213*	-1 15 44	Supp Motor Area L	SAL
215*	0 -30 27	Cingulum Ant L	SAL
ROI	nback-fMRI		
47*	-3 2 53	Supp Motor Area L	CNG
57	-34 3 4	Clausrum	CNG
59*	-5 18 34	Cingulum Mid L	CNG
112*	-2 38 36	Frontal Sup Medial L	DMN
113*	-3 42 16	Cingulum Ant L	DMN
145	8 -72 11	Cakcarine R	VIS
153*	43 -78 -12	Occipital Inf R	VIS
162*	24 -87 24	Occipital Sup R	VIS
167*	-3 -81 21	Cuneus L	VIS
202	-3 26 44	Frontal Sup Medial L	FPN
213*	-1 15 44	Supp Motor Area L	SAL
215*	0 30 27	Cingulum Ant L	SAL
229	31 -14 2	Putamen R	SCT

* indicates the ROIs common to emoid-fMRI and nback-fMRI

¹ the coordinates of the ROIs' center point in Montreal Neurological Institute space and the anatomical regions [26] that the ROI locates in.

1) *ROI identification*: We applied Grad-RAM to identify the ROIs, which played essential roles in WRAT prediction. The Grad-RAM values $\alpha^{(m)}$ for 264 ROIs were further normalized by Z-score normalization. Next, we reported the visualization results separately for each fMRI paradigm. Specifically, we considered the top 5% ROIs with the largest Grad-RAM values and further analyzed the FN segregation with the selected ROIs in Table IV. In addition, the BrainNetViewer [30] was used to visualize the ROI identification results in anatomical space, shown in Fig.6.

2) *FC identification*: Moreover, we interpreted our model by identifying the significant cognition-related FCs using edge mask learning. Because two fMRI paradigms were mapped using the same brain template, we only investigated a single edge mask for both fMRI paradigms. For edge mask learning, the model was retrained using all subjects until the loss function in Eq.15 converged. We remain all other hyperparameters the same as the previous experiment and set the L_1 regularization parameters β in a grid of $\{0.05, 0.1, 0.5, 1, 5, 10\}$ to control the sparsity of the edge mask. For each value in the grid, we trained the model to learn the mask matrices for 10 times. The edge mask matrices were first binarized that we set the positive elements to 1 and other non-positive entries to 0.

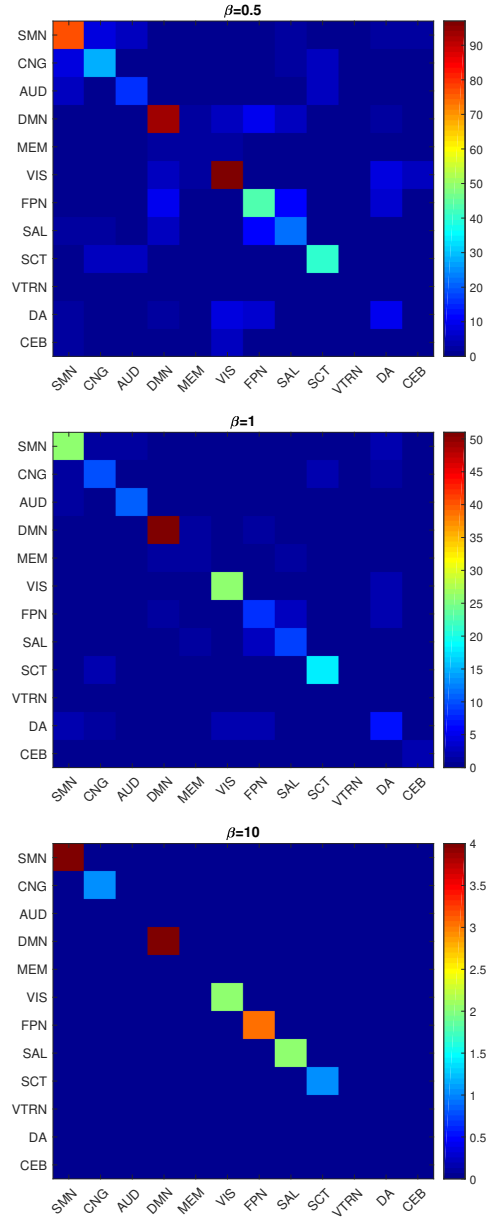


Fig. 5. Module allegiance matrices with different L_1 regularization parameters

Then, we calculated the frequency of the appearance for each FC and showed the binary edge mask with a threshold of 0.5 in Fig.4. We selected β based on the sparsity of the edge mask. Consequently, we set β 0.5 and 1 with the sparsity of the edge mask between 5% and 1%, shown in Fig.3. Next, we qualitatively analyzed the FN integration by constructing the module allegiance matrices [31] and calculating the numbers of FCs for different β within each FN and between each pair of FNs. The pair of FNs with large value in the module allegiance matrix suggests that two FNs may be part of the same function-related community, shown in Fig.5.

E. Discussion

In this work, we used a proposed MGCN framework to predict the WRAT scores using both emotion and nback fMRI.

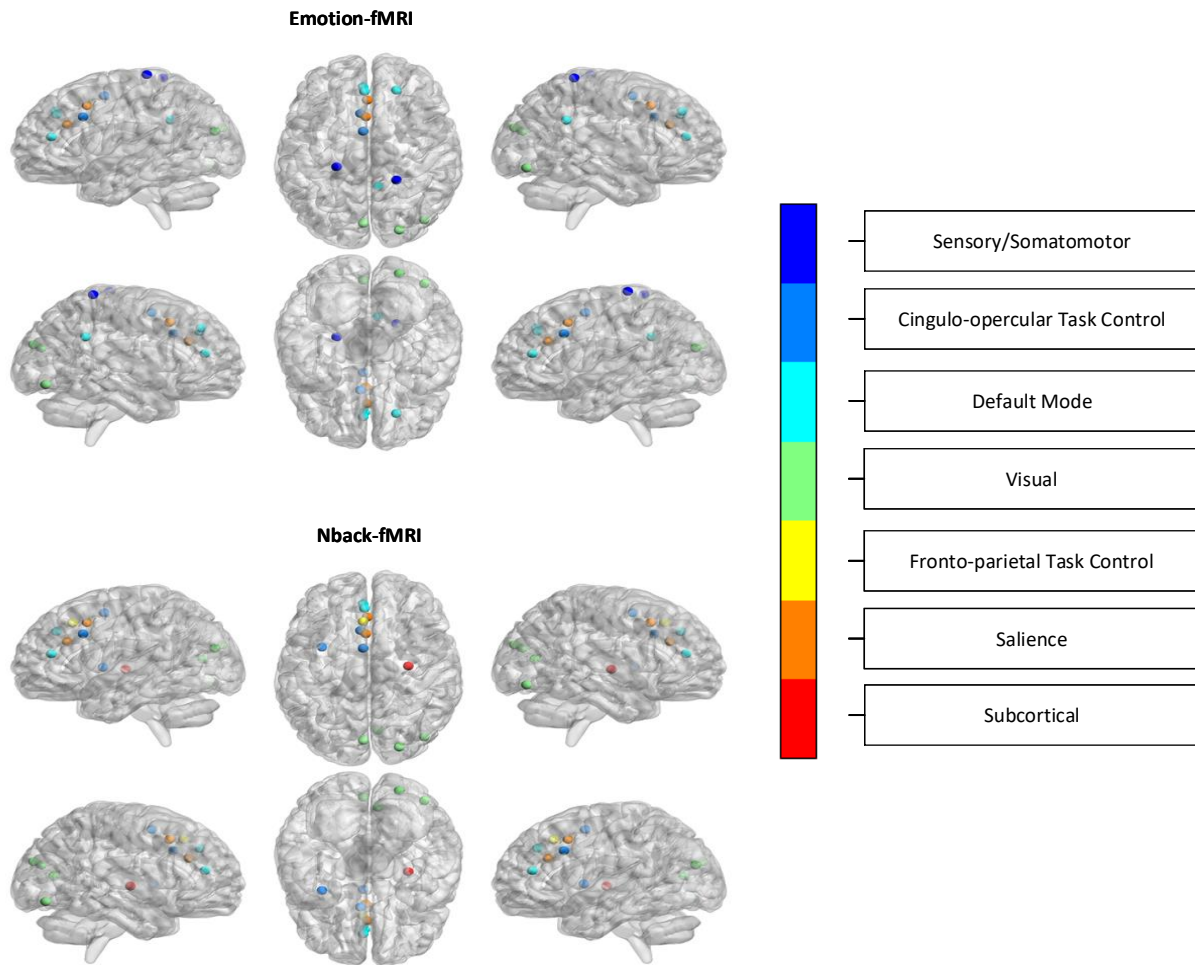


Fig. 6. The figure shows the anatomical view of selected ROIs (5%) based on the power264 template. The same color indicates that the ROIs are in the same functional network. The upper parts are the results for emotion-fMRI; the lower parts are the results for nback-fMRI. Each figure contains the views from different layouts (sagittal, axial, coronal).

We validated our model on the PNC dataset and compared our approach with other methods. The results showed that our MGCN got significantly improved predictive performance over GCN as well as the other competing approaches. Next, we applied Grad-RAM and edge mask learning to interpret our model and identify the significant ROIs and FCs, which played significant roles in predicting WRAT scores. Based on the results of ROI identification, we further measured the brain segregation and identified 7 FNs related to human cognitive variability. The cognition-related functions of these FNs were reported by previous studies based on different measures.

- **SMN**: According to the study in [32], [33], the recruitment of the bilateral postcentral gyrus from SMN, which is also identified by our MGCN (23 Postcentral L and 32 Postcentral R), plays a significant role in multiple cognitive processes, such as verbal creativity, memory retrieval, imaginative process, cognitive control.
- **CNG**: The CNG network, which is associated with output gating of memory, plays a more downstream role in cognitive control and maintaining cognitive faculties available for current processing requirements [34], [35].
- **DMN**: Based on the anatomical structure, DMN locates at the top of a cortical hierarchy and is relatively isolated from systems directly involved in perception and action, which suggests it plays an integrative role in cognition [36], [37]. More evidence [36], [38] shows that DMN performs the significant function of navigating social interaction, planning for the future using the experiences.
- **VIS**: During some specific learning processes, there is communication among visual cortex regions in the early sessions when subjects are still getting familiar with the visual cues and do not register high rates of task completion [39]. Another possible reason for the identification of the visual network may be the scenario of collecting data [16], [17]. When the fMRI data was collected, the subjects were asked to fixate their eyes on the crosshair, which may involve the recruitment of visual networks.
- **FPN**: Based on recent studies [35], [40], as a flexible hub of cognitive control, FRN can not only reflect the commitment of specific tasks but also serve as a code that can promote learning novel tasks.
- **SAL**: According to the study in [41]–[43], the SAL

can perform multiple complex brain cognitive functions, including self-awareness, emotional, and cognitive information.

- **SCT:** Studies in [44], [45] show that the subcortical network has a pivotal role in human cognitive, affective, and social functions. SCT also associates with human language control [46].

In addition, we identified the FC functioned most significantly in the cognition-related task using edge mask learning. Results are shown in Fig.5:

- The segregation of distinct networks with stronger within FNs and weaker between FNs connectivity can be observed with a larger β value.
- When increasing β to 10, only the diagonal element remained in the mask. Thus, the model identified the most significant cognition-related FNs, including SMN, CNG, DMN, VIS, FPN, SAL, SCT, which are identical with the identification results obtained by the Grad-RAM approach. These results cross-validated the effectiveness of both model interpretation approaches.
- We observed high integration between FPN and SAL. A strong relationship between these two FNs has been reported in the previous study [47], suggesting that the FPN may be part of the SAL [47]. Specifically, FPN and SAL respond to the salient environmental stimuli, stimulating the cascade of cognitive control signals [43] and collaborating for the better task accuracy [48].
- The integration between DMN and FPN can be observed from our results. Studies suggest that the integration between DMN and FPN contributes to the mind-wandering state associating with cognitive control [49], [50].

IV. CONCLUSION

In this paper, we proposed an interpretable MGCN model for the joint analysis of multi-modal data. To simultaneously incorporate the relationships of subjects within and between modalities, we enforced a manifold based regularization term. We validated our proposed model on the PNC dataset by using multiple paradigms of fMRI. The experimental results demonstrated the superior prediction performance compared with other competing models, indicating that the MGCN can efficiently learn the graph embeddings from multi-modal data and boost the prediction performance. In addition, we proposed Grad-RAM and edge mask learning to qualitatively interpret our model at different levels and identify the significant cognition-related biomarkers. The results from Grad-RAM and the edge mask learning cross-validated one another. The identified biomarkers are supported by the previous reports and may partially account for the variance in human cognitive function.

REFERENCES

- [1] E. Adeli *et al.*, "Multi-task prediction of infant cognitive scores from longitudinal incomplete neuroimaging data," *NeuroImage*, vol. 185, pp. 783–792, 2019.
- [2] V. D. Calhoun and J. Sui, "Multimodal fusion of brain imaging data: a key to finding the missing link (s) in complex mental illness," *Biological psychiatry: cognitive neuroscience and neuroimaging*, vol. 1, no. 3, pp. 230–244, 2016.
- [3] M. S. Cetin *et al.*, "Thalamus and posterior temporal lobe show greater inter-network connectivity at rest and across sensory paradigms in schizophrenia," *Neuroimage*, vol. 97, pp. 117–126, 2014.
- [4] V. D. Calhoun *et al.*, "A method for multitask fmri data fusion applied to schizophrenia," *Human brain mapping*, vol. 27, no. 7, pp. 598–610, 2006.
- [5] J. Sui *et al.*, "Discriminating schizophrenia and bipolar disorder by fusing fmri and dti in a multimodal cca+ joint ica model," *Neuroimage*, vol. 57, no. 3, pp. 839–855, 2011.
- [6] B. Jie *et al.*, "Manifold regularized multitask feature learning for multimodality disease classification," *Human brain mapping*, vol. 36, no. 2, pp. 489–507, 2015.
- [7] X. Zhu *et al.*, "A novel relational regularization feature selection method for joint regression and classification in ad diagnosis," *Medical image analysis*, vol. 38, pp. 205–214, 2017.
- [8] L. Xiao *et al.*, "A manifold regularized multi-task learning model for iq prediction from two fmri paradigms," *IEEE Transactions on Biomedical Engineering*, vol. 67, no. 3, pp. 796–806, 2019.
- [9] T. N. Kipf and M. Welling, "Semi-Supervised Classification with Graph Convolutional Networks," in *Proceedings of the 5th International Conference on Learning Representations*, ser. ICLR '17, 2017. [Online]. Available: <https://openreview.net/forum?id=SJU4ayYgl>
- [10] S. Parisot *et al.*, "Disease prediction using graph convolutional networks: Application to autism spectrum disorder and alzheimer's disease," *Medical image analysis*, vol. 48, pp. 117–130, 2018.
- [11] X. Li *et al.*, "Graph neural network for interpreting task-fmri biomarkers," in *International Conference on Medical Image Computing and Computer-Assisted Intervention*. Springer, 2019, pp. 485–493.
- [12] V. D. Calhoun *et al.*, "The chronectome: time-varying connectivity networks as the next frontier in fmri data discovery," *Neuron*, vol. 84, no. 2, pp. 262–274, 2014.
- [13] R. R. Selvaraju *et al.*, "Grad-cam: Visual explanations from deep networks via gradient-based localization," in *Proceedings of the IEEE International Conference on Computer Vision*, 2017, pp. 618–626.
- [14] A. Chattopadhyay *et al.*, "Grad-cam++: Generalized gradient-based visual explanations for deep convolutional networks," in *2018 IEEE Winter Conference on Applications of Computer Vision (WACV)*. IEEE, 2018, pp. 839–847.
- [15] Z. Wang and J. Yang, "Diabetic retinopathy detection via deep convolutional networks for discriminative localization and visual explanation," in *Workshops at the Thirty-Second AAAI Conference on Artificial Intelligence*, 2018.
- [16] T. D. Satterthwaite *et al.*, "Neuroimaging of the philadelphia neurodevelopmental cohort," *Neuroimage*, vol. 86, pp. 544–553, 2014.
- [17] T. D. Satterthwaite *et al.*, "The philadelphia neurodevelopmental cohort: A publicly available resource for the study of normal and abnormal brain development in youth," *Neuroimage*, vol. 124, pp. 1115–1119, 2016.
- [18] R. A. Test, "Wide range achievement test 4 (wrat4)," *Journal of Occupational Psychology, Employment and Disability*, vol. 11, no. 1, p. 49, 2009.
- [19] J. Bruna, W. Zaremba, A. Szlam, and Y. Lecun, "Spectral networks and locally connected networks on graphs," in *International Conference on Learning Representations (ICLR2014)*, CBLIS, April 2014, 2014, pp. <http://openreview>.
- [20] G. Wilkinson and G. Robertson, "Wide range achievement test 4 professional manual: Psychological assessment resources," 2006.
- [21] P. Zille *et al.*, "Enforcing co-expression within a brain-imaging genomics regression framework," *IEEE transactions on medical imaging*, vol. 37, no. 12, pp. 2561–2571, 2017.
- [22] J. Fang *et al.*, "Fast and accurate detection of complex imaging genetics associations based on greedy projected distance correlation," *IEEE transactions on medical imaging*, vol. 37, no. 4, pp. 860–870, 2017.
- [23] K. J. Friston *et al.*, "Characterizing dynamic brain responses with fmri: a multivariate approach," *Neuroimage*, vol. 2, no. 2, pp. 166–172, 1995.
- [24] J. D. Power *et al.*, "Functional network organization of the human brain," *Neuron*, vol. 72, no. 4, pp. 665–678, 2011.
- [25] J. D. Power *et al.*, "Methods to detect, characterize, and remove motion artifact in resting state fmri," *Neuroimage*, vol. 84, pp. 320–341, 2014.
- [26] J. D. Schmahmann *et al.*, "Three-dimensional mri atlas of the human cerebellum in proportional stereotaxic space," *Neuroimage*, vol. 10, no. 3, pp. 233–260, 1999.
- [27] J. Bergstra and Y. Bengio, "Random search for hyper-parameter optimization," *The Journal of Machine Learning Research*, vol. 13, no. 1, pp. 281–305, 2012.
- [28] A. Argyriou *et al.*, "Multi-task feature learning," in *Proceedings of the 19th International Conference on Neural Information Processing Systems*, 2006, pp. 41–48.

- [29] X. Zhang *et al.*, “Multi-view graph convolutional network and its applications on neuroimage analysis for parkinson’s disease,” in *AMIA Annual Symposium Proceedings*, vol. 2018. American Medical Informatics Association, 2018, p. 1147.
- [30] M. Xia *et al.*, “Brainnet viewer: a network visualization tool for human brain connectomics,” *PloS one*, vol. 8, no. 7, p. e68910, 2013.
- [31] M. G. Mattar *et al.*, “A functional cartography of cognitive systems,” *PLoS computational biology*, vol. 11, no. 12, p. e1004533, 2015.
- [32] Q. Feng *et al.*, “Verbal creativity is correlated with the dynamic reconfiguration of brain networks in the resting state,” *Frontiers in psychology*, vol. 10, p. 894, 2019.
- [33] S. Chenji *et al.*, “Investigating default mode and sensorimotor network connectivity in amyotrophic lateral sclerosis,” *PLoS One*, vol. 11, no. 6, 2016.
- [34] S. Sadaghiani and M. D’Esposito, “Functional characterization of the cingulo-opercular network in the maintenance of tonic alertness,” *Cerebral Cortex*, vol. 25, no. 9, pp. 2763–2773, 2015.
- [35] G. Wallis *et al.*, “Frontoparietal and cingulo-opercular networks play dissociable roles in control of working memory,” *Journal of Cognitive Neuroscience*, vol. 27, no. 10, pp. 2019–2034, 2015.
- [36] M. D. Fox *et al.*, “The human brain is intrinsically organized into dynamic, anticorrelated functional networks,” *Proceedings of the National Academy of Sciences*, vol. 102, no. 27, pp. 9673–9678, 2005.
- [37] R. BUCKNER *et al.*, “The brain’s default network: Anatomy, function, and relevance to disease,” *Annals of the New York Academy of Sciences*, vol. 1124, no. 1, pp. 1–38, 2008.
- [38] M. Sormaz *et al.*, “Default mode network can support the level of detail in experience during active task states,” *Proceedings of the National Academy of Sciences*, vol. 115, no. 37, pp. 9318–9323, 2018.
- [39] P. Bogdanov *et al.*, “Learning about learning: Mining human brain sub-network biomarkers from fmri data,” *PloS one*, vol. 12, no. 10, 2017.
- [40] T. P. Zanto and A. Gazzaley, “Fronto-parietal network: flexible hub of cognitive control,” *Trends in cognitive sciences*, vol. 17, no. 12, pp. 602–603, 2013.
- [41] A. W. Toga, *Brain mapping: An encyclopedic reference. Volume 1+ 2+ 3*. Academic Press, 2015.
- [42] A. D. Craig and A. Craig, “How do you feel—now? the anterior insula and human awareness,” *Nature reviews neuroscience*, vol. 10, no. 1, 2009.
- [43] V. Menon and L. Q. Uddin, “Saliency, switching, attention and control: a network model of insula function,” *Brain Structure and Function*, vol. 214, no. 5-6, pp. 655–667, 2010.
- [44] D. Koshiyama *et al.*, “Role of subcortical structures on cognitive and social function in schizophrenia,” *Scientific reports*, vol. 8, no. 1, pp. 1–9, 2018.
- [45] J. Wu *et al.*, “Brain network reconfiguration for language and domain-general cognitive control in bilinguals,” *NeuroImage*, vol. 199, pp. 454–465, 2019.
- [46] K. A. Bridges *et al.*, “The role of subcortical structures in recited speech: Studies in parkinson’s disease,” *Journal of neurolinguistics*, vol. 26, no. 6, pp. 591–601, 2013.
- [47] W. W. Seeley *et al.*, “Dissociable intrinsic connectivity networks for salience processing and executive control,” *Journal of Neuroscience*, vol. 27, no. 9, pp. 2349–2356, 2007.
- [48] A. Elton and W. Gao, “Divergent task-dependent functional connectivity of executive control and salience networks,” *Cortex*, vol. 51, pp. 56–66, 2014.
- [49] K. C. Fox *et al.*, “The wandering brain: Meta-analysis of functional neuroimaging studies of mind-wandering and related spontaneous thought processes,” *Neuroimage*, vol. 111, pp. 611–621, 2015.
- [50] J. Golchert *et al.*, “Individual variation in intentionality in the mind-wandering state is reflected in the integration of the default-mode, frontoparietal, and limbic networks,” *Neuroimage*, vol. 146, pp. 226–235, 2017.